JOURNAL OF SPACECRAFT AND ROCKETS
Vol. 43, No. 5, September–October 2006

Global/Local Analysis Strategy for Partly Wrinkled Membrane

Kyeongsik Woo*
Chungbuk National University, Cheongju, Chungbuk 361-763, Republic of Korea
and
Christopher H. Jenkins†
Montana State University, Bozeman, Montana 59717-3800

DOI: 10.2514/1.18603

In this study, a global/local analysis strategy for partly wrinkled membranes is presented. In the global analysis, a relatively coarse membrane element mesh is used to calculate in-plane displacements and stresses. The local shell analyses are then performed selectively for the wrinkled region to calculate the detailed wrinkle deformation. Solutions from the global model are used to derive the boundary conditions for the local model. In the global analysis, the penalty-parameter modified material modeling approach is employed for wrinkled membranes. The wrinkle deformation is obtained from a local nonlinear post-buckling shell analysis using refined meshes seeded with random geometric imperfection. In the numerical calculation, the global/local analysis procedure is illustrated for a corner-loaded square membrane. The accuracy of the global/local procedure is established by comparing the results with those of conventional shell analysis, and the mesh convergence and global/local boundary conditions are also studied.

Nomenclature

D_{ij}	=	stiffness
D^*_{ij}	=	modified stiffness
E	=	Young's modulus
P	=	penalty parameter
S_{ij}	=	compliance
T_1, T_2	=	corner loads
t	=	membrane thickness
u, v, w	=	displacements
Γ_T, Γ_W	=	taut and wrinkled boundaries
$\varepsilon_{\max}, \varepsilon_{\min}$	=	major and minor principal strains
$\theta_x, \theta_y, \theta_z$	=	rotation degrees of freedom
ν	=	Poisson's ratio
$\sigma_{\max}, \sigma_{\min}$	=	major and minor principal stresses

I. Introduction

RECENTLY, thin membranes have been extensively considered for use in lightweight gossamer space structures. Thin membranes are exceptionally light in mass and can be packaged into very small volumes. Having vanishingly small bending stiffness, however, they buckle almost immediately when subjected to compressive stress, which is called wrinkling. Along with large displacement behavior due to the underconstrained nature of thin membrane structural system, the wrinkling behavior provides a major computational challenge.

In the finite element analysis of membrane wrinkling, two approaches have been developed. The first is to use membrane elements and predict fictitious smooth surface that accounts for the wrinkle deformation in an averaged sense. Roddeman et al. [1–3] employed the modification of the deformation tensor to obtain the smooth surface that produced the correct stress state of a membrane after wrinkling. This method was further developed by other researchers (e.g., [4–6]) to study the behavior of wrinkled membranes. The averaged wrinkle deformation was also obtained by modifying material properties. For this, Miller et al. [7] applied Poisson's ratio modification, and Miyazaki and Nakamura [8] and Liu et al. [9] developed stiffness/compliant matrix modification modeling to simulate the compression free wrinkle state. The latter has been successfully implemented to the commercial FEM code ABAQUS as a user subroutine.

Another approach to the membrane wrinkling problem is to perform nonlinear post-buckling analysis using thin shell elements and explicitly predict the detailed wrinkle deformation. In this case, the shell element meshes are seeded with initial geometrical imperfection to instigate the out-of-plane deformation. Wong et al. [10] and Su et al. [11] performed eigenvalue analysis first, and then used a combination of several eigenmodes as the imperfection. Tessler et al. [12] obtained the wrinkle deformation initiated by random imperfection.

For very thin membranes, the out-of-plane stress components are negligible and only the in-plane stress components are important. Thus, from a strength point of view, often the membrane element analysis suffices. This, however, cannot offer any detailed wrinkle information in the out-of-plane direction, which is needed, for example, when one tries to investigate the effect of wrinkles on solar sail thrust performance [13] and control [14]. The shell analysis, though providing detailed wrinkle information, can be very costly. To have reasonable wrinkle shapes, one has to use refined meshes with a large number of nodes. In addition, the wrinkling can occur in high frequency modes, which can only be represented by highly refined meshes, requiring huge computer resources.

In this study, a global/local analysis strategy for partly wrinkled thin membranes is presented. In the global analysis, a relatively coarse membrane element mesh is used to calculate in-plane displacements and stresses. The wrinkled region is also predicted in this analysis. The local shell analyses are performed selectively for the wrinkled region to calculate the detailed wrinkle deformation. Solutions from the global model are used to derive the boundary conditions for the local model. In the global analysis, the penalty-parameter modified material modeling approach [9] is employed for the wrinkled membrane. The wrinkle deformation is obtained from a local nonlinear post-buckling shell analysis using refined meshes seeded with random geometric imperfection.

Presented as Paper 1977 at the 46th AIAA/ASME/ASCE/AHS/ASC Structures, Structural Dynamics and Materials Conference, Austin, Texas, 18–22 April 2005; received 7 July 2005; revision received 3 March 2006; accepted for publication 15 March 2006.

*Professor, Department of Structural Systems & CAE. Member AIAA.
†Professor and Head, Department of Mechanical and Industrial Engineering, 220 Robert Hall, P.O. Box 173800. Associate Fellow AIAA.

In the following, the global/local analysis procedure is first described, with the derivation of the local boundary conditions (LBC). Then, it is illustrated using a square membrane model in predicting the wrinkle deformation. The procedure is investigated to establish its accuracy by comparing the results with those of conventional shell analysis. The effects of global/local boundary conditions, membrane thickness, and applied load level on the wrinkling behavior are also presented.

II. Global/Local Analysis

Global/local finite element analysis is often used to study the stress distribution in a small portion of structures in great detail. There are several forms in the global/local method in the literature (e.g., [15–17]). The global/local analysis procedure employed in this study uses separate meshes: a relatively crude global membrane element mesh to obtain the overall response of the structure and refined local shell element meshes to obtain the detailed wrinkle deformation shapes.

Figure 1 shows the procedure of defining of local region and global/local boundary conditions for a corner-loaded square membrane. First, a global analysis is performed to predict the wrinkled region. For this, a membrane element mesh is used with the wrinkle subroutine by the penalty-parameter modified material model [9]. In Fig. 1a, the wrinkled region is plotted. Here, the element is color-coded as taut, partly wrinkled, or wrinkled as per the stress/strain states at the integration points of the element. In this figure, one can see that under the unsymmetric loading condition localized wrinkling occurred near the corner regions, with two corners having larger wrinkled area. At this point, all the in-plane solutions needed for structural design become available.

To obtain the detailed wrinkle deformation, one could remodel the whole membrane with shell elements and perform post-buckling analysis. For partly wrinkled membrane problems like the one shown in Fig. 1a, however, the detailed shell analysis is needed only for the region where the wrinkling is predicted to occur. In this case, one can identify the local regions of interest, model the region with refined shell elements, and perform the analysis. This is done by the following procedure:

1) Perform global analysis using membrane elements.

2) From the distribution of wrinkled region predicted by the global solution, identify and model the region(s) of interest with refined shell elements.

3) Derive local boundary conditions from the global solution and apply these to the local mesh.

4) Perform geometrically nonlinear post-buckling analysis for the local shell mesh.

Figure 1b shows that the global/local boundary can be divided into taut and wrinkled boundaries from the global solution. The in-plane displacement boundary conditions are directly derived from the global solutions. However, more consideration is needed to specify the rest of the local boundary conditions due to the incompatibility of degrees of freedom, because different element types with different number of degrees of freedom are used in the global and local analyses. In this study, it is thought that the w-displacement can be constrained to be zero for the nodes in the taut boundary, whereas it is unconstrained for those in the wrinkled boundary. The same reasoning can be applied to the rotations. However, preliminary study showed boundary conditions on the rotation degrees of freedom do not have significant effect when thickness is small, thus they are all set free herein. In short, the global/local boundary conditions used are:

1) In-plane displacements (u, v) calculated from the global solution are specified on $\Gamma_T + \Gamma_W$.

2) Out-of-plane displacements (w) are constrained on Γ_T, and unconstrained on Γ_W.

3) All rotations ($\theta_x, \theta_y, \theta_z$) are unconstrained on $\Gamma_T + \Gamma_W$.

In this study, other boundary conditions were considered and the effect of boundary conditions on the wrinkling is discussed in Sec. IV. The preceding boundary condition is named as LBC1 for distinction.

It should also be noted that because the local mesh usually has much higher mesh density than the global mesh, there is no one-to-one match between the global and local nodes at the global/local boundary. In this study, cubic spline interpolation of the global in-plane displacements was performed to calculate the displacements for the local boundary nodes.

III. Finite Element Meshes

The global/local analysis strategy was applied to a square membrane. Figure 2 shows the configuration of a 500×500 mm square membrane loaded at the corners through cables. The material properties are $E = 3.5$ GPa, $\nu = 0.3$, and the thickness is 10 μm. The corners are cut off with the edge length of 14 mm and 1.5-mm-diam steel pins are attached to spread the load. The loads are applied at the tip of 1-mm-diam Kevlar cables with the elastic modulus of 70.3 GPa. The length of the cables is 49.5 mm.

The square membrane was analyzed using ABAQUS. It was modeled with membrane elements (M3D4/M3D3) in the global meshes (GM), and shell elements (S4R5/S3R) in the local meshes (LM). For comparison, the whole membrane was also modeled with shell elements and named as conventional meshes (CM). In all cases, the steel pins were modeled with beams (B31), and cables with rods (T3D2).

Figure 3 shows example global and local meshes. The local mesh in Fig. 3b is for the region marked by the dotted line in the global mesh in Fig. 3a. Tables 1 and 2 summarize the number of elements. Note that the global membrane meshes are the same in shape as the conventional ones but differ in element types, thus the mesh information is only listed for the latter in Table 1. The meshes are numbered in such a way that CM*i*s and LM*i*s are the same in element sizes, i.e., have the same mesh density in the local region. The global mesh GM1 in Fig. 3a corresponds to CM1 with replacing shells by membranes in element types. The largest local mesh considered was LM9 modeled with 87,132 shell elements. It would require a prohibitively large number of more than 700,000 shell elements if

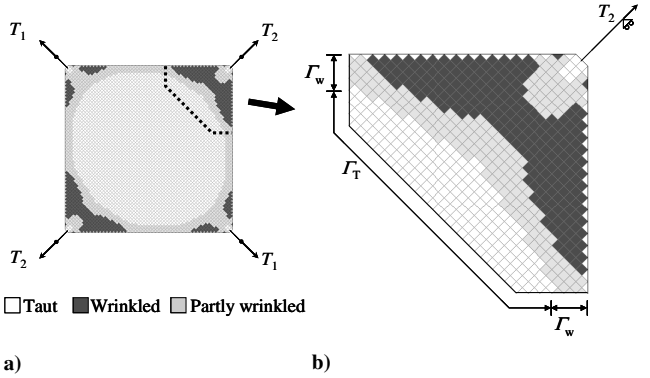

Fig. 1 Defining the local region: a) wrinkled area and b) definition of local boundaries ($E = 3.5$ GPa, $\nu = 0.3$, $t = 10$ μm, $T_1 = 22.5$ N, $T_2 = 30$ N).

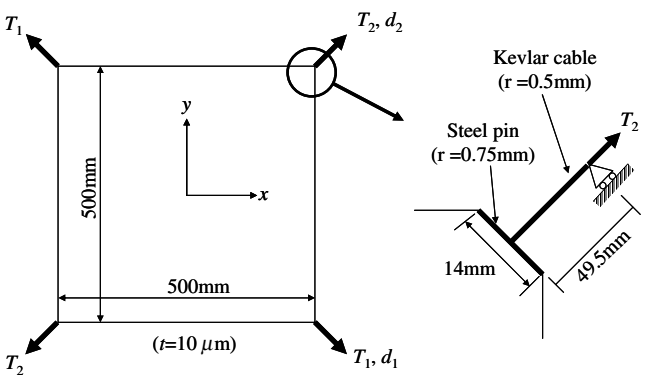

Fig. 2 Corner-loaded square membrane.

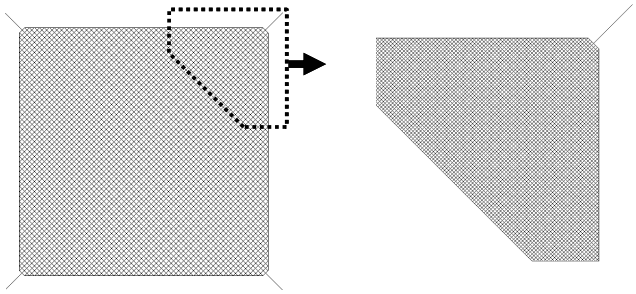

Fig. 3 Example meshes: a) global (GM1) and b) local (LM3).

one should try modeling a conventional mesh with the same mesh density.

IV. Numerical Results

As described previously, the global analysis was performed using membrane element meshes, in which the wrinkling was accounted for by the penalty-parameter modified material modeling approach. The detailed wrinkle deformation was obtained from local nonlinear post-buckling analyses with refined shell element meshes. To instigate wrinkling, the meshes were seeded with random geometric imperfection [12], and *STATIC, STABILIZE option was used to stabilize the solution procedure in ABAQUS.

A. Comparison of Conventional vs Global/Local Results

Figure 4 compares the global/local and conventional deformed meshes for the 10 μm thickness square membrane when the applied loads were $T_1 = 22.5$ N and $T_2 = 30$ N. The figure shows the wrinkle deformation at the T_2-corner, which was the upper-right corner in Fig. 1. (In fact, Fig. 1 shows the distribution of wrinkled elements by the global analysis for the current load condition.) In this figure, only the out-of-plane displacement component was plotted for better viewing. The results were obtained using GM1 + LM5, i.e., 5092 membrane, 8 beam, and 1 rod elements for the global analysis, and 15,200 shell, 10 beam, and 1 rod elements for the local analysis. The conventional shell analysis was also performed for comparison using 125,380 shell, 40 beam, and 4 rod elements (CM5). (This clearly indicates that the global/local analysis saved computational resources significantly.) For fair comparison, the

Table 1 Number of elements: conventional mesh

	S4R5/S3R	B31	T3D2
CM1	5,092	8	4
CM2	20,176	16	4
CM3	45,252	24	4
CM4	80,320	32	4
CM5	125,380	40	4

Table 2 Number of elements: local mesh

	S4R5/S3R	B31	T3D2
LM1	628	2	1
LM2	2,462	4	1
LM3	5,502	6	1
LM4	9,748	8	1
LM5	15,200	10	1
LM6	21,858	12	1
LM7	38,792	16	1
LM8	60,550	20	1
LM9	87,132	24	1

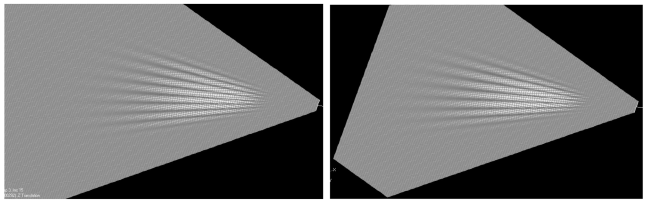

a) b)

Fig. 4 Comparison of wrinkle shapes: a) conventional and b) global/local.

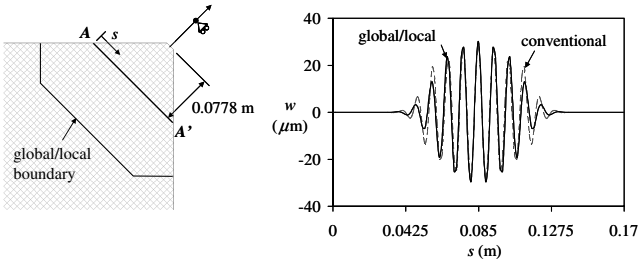

a) b)

Fig. 5 Comparison of wrinkle displacements along AA' line: a) definition of AA' line, and b) wrinkle displacements.

mesh density of the local mesh was kept to be the same as that of the conventional mesh. For both the conventional and local meshes, random geometrical imperfection with the magnitude of 0.01% of the membrane thickness was applied to the internal nodes. As can be seen in Fig. 4, the wrinkle deformation shapes obtained by the global/local analysis were in excellent agreement with that of the conventional analysis. The wrinkle pattern and wrinkled region matched very well. For better comparison, the out-of-plane displacement was plotted along the AA' line crossing the middle of the local region in Fig. 5. (The AA' line is defined in Fig. 5a, where the distance along the AA' line is denoted by s.) These results indicate that the global/local analysis predicted the detailed wrinkle displacements very accurately. The difference in the maximum wrinkle heights between the global/local and conventional analyses was only 3.34%.

B. Mesh Convergence Study

The mesh convergence analyses were performed for the global/local meshes. This was done for 10 μm and 2 μm thickness models. For the 2 μm thickness model, the applied loads were scaled accordingly to $T_1 = 4.5$ N and $T_2 = 6$ N. The steel pin and cable diameters were kept the same as the 10 μm thickness model.

Figure 6 shows the convergence of the w-displacements along the AA' line. These were calculated using GM1 + LMi meshes. As can be seen in this figure, good convergence was obtained even with moderately refined local meshes for the 10 μm thickness model. However, the convergence was much slower for the 2 μm thickness model. The convergence was not achieved until the use of very refined meshes of LM8 and LM9. This was due to the increase in the number of wrinkles as the thickness decreased that required a large number of elements to represent the fine details of the wrinkle deformation.

Figure 7 shows the contour plots of wrinkle deformation shape for the models with different thicknesses. These were calculated using GM1 + LM9 meshes. As was seen in Fig. 6, a much finer and wider wrinkle pattern occurred as the membrane became thinner, which clearly indicated the thinner membrane required highly refined meshes for convergence. In addition, one can observe that unlike the 10 μm thickness membrane, the 2 μm thickness membrane had wrinkle pattern fanning out from the edges of the steel pin attached to spread the load, and thus, had two maximum wrinkle peaks occur

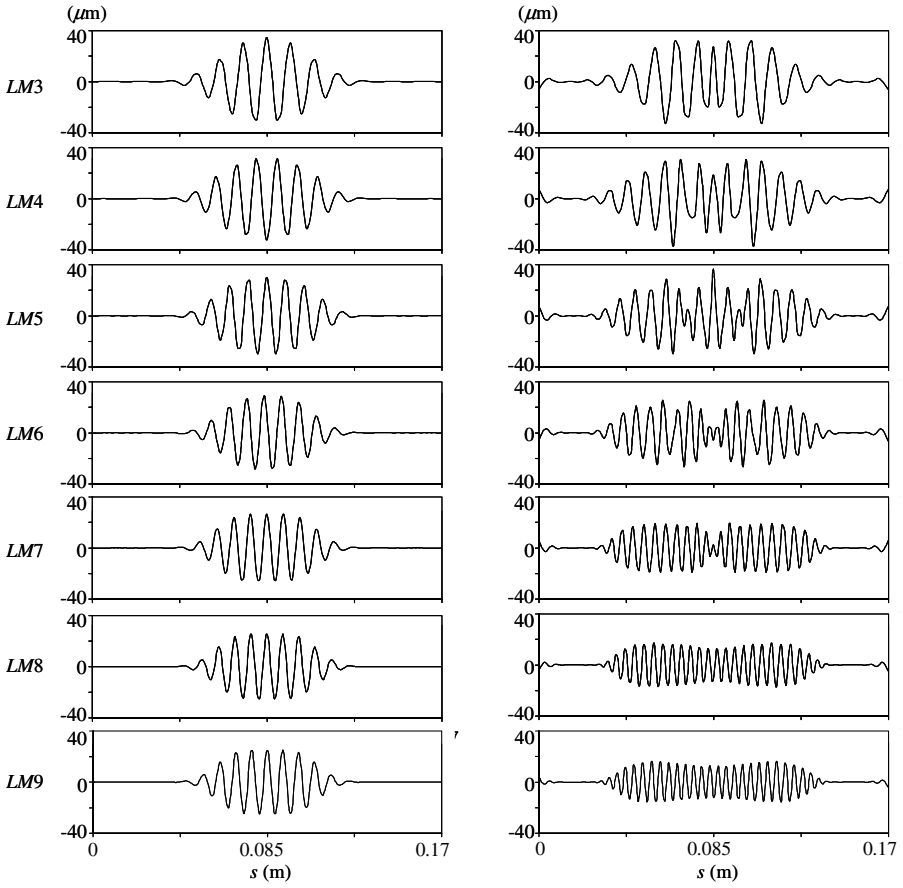

Fig. 6 Convergence of wrinkle displacements along the AA' line: a) $t = 10$ μm and b) $t = 2$ μm.

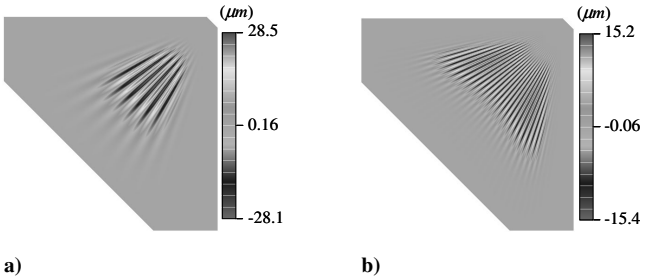

Fig. 7 Contour plots of wrinkle displacements for models with different thicknesses: a) $t = 10$ μm and b) $t = 2$ μm.

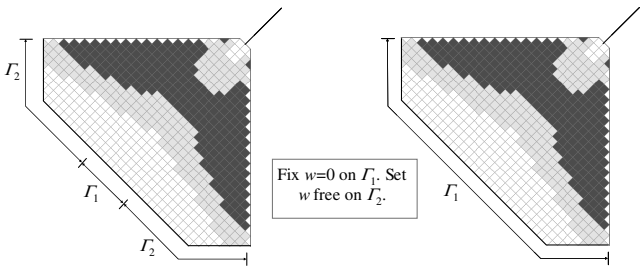

Fig. 8 Definition of global/local boundaries: a) LBC2 and b) LBC3.

away from the diagonal region of the membrane, i.e., the midpoint of the AA' line. This can be seen more clearly from Fig. 6, and indicated that the wrinkle pattern of the 2 μm thickness membrane was more sensitive to how the load was applied. Note that the shape of the wrinkled region of the thinner model became more similar to that predicted by the global analysis with wrinkle modeling (see Fig. 1b).

C. Effects of Boundary Conditions on Global/Local Results

The effect of global/local boundary conditions was investigated. In addition to the boundary condition LBC1 described in Sec. II, we considered two more boundary conditions LBC2 and LBC3 as shown in Fig. 8. This was to try constraining less or more of the out-of-plane displacement at the global/local boundary. As in LBC1, the

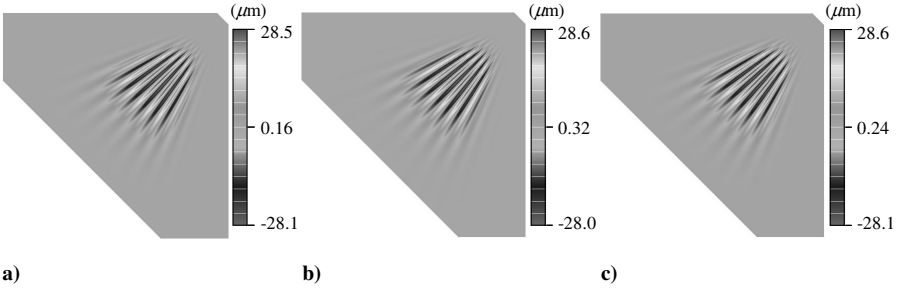

Fig. 9 Contour plots of wrinkle displacements with different boundary conditions for 10 μm thickness model: a) LBC1, b) LBC2, and c) LBC3.

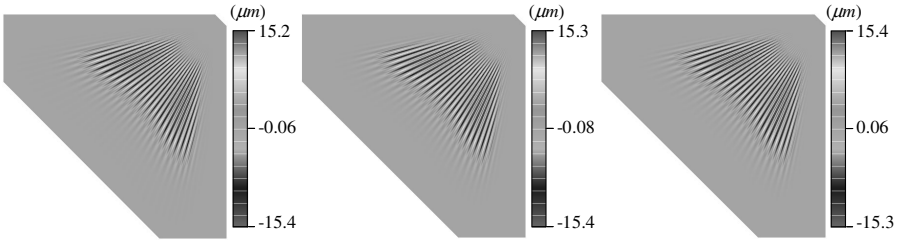

a) b) c)

Fig. 10 Contour plots of wrinkle displacements with different boundary conditions for 2 μm thickness model: a) LBC1, b) LBC2, and c) LBC3.

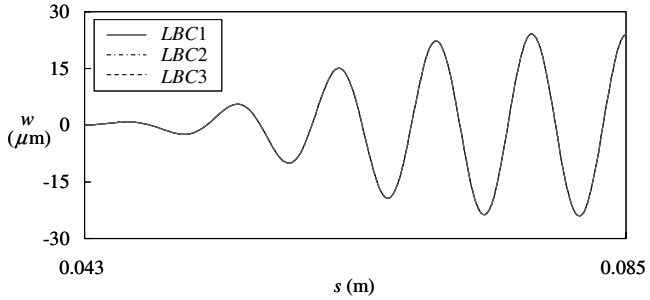

Fig. 11 Comparison of wrinkle displacements along AA' line with different boundary conditions for 10 μm thickness model.

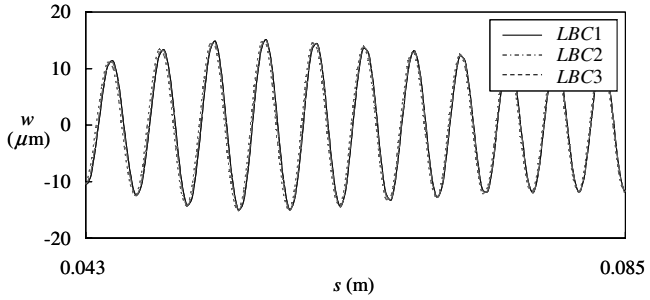

Fig. 12 Comparison of wrinkle displacements along AA' line with different boundary conditions for 2 μm thickness model.

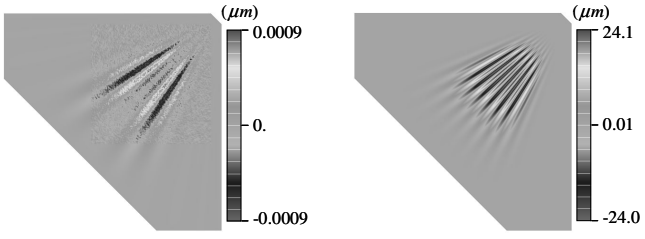

a) b)

Fig. 13 Contour plots of wrinkle displacements at different load levels for 10 μm thickness model: a) $T_1 = 22.5$ N, $T_2 = 3$ N; and b) $T_1 = 22.5$ N, $T_2 = 30$ N.

in-plane displacements were interpolated from the global membrane solution and the all rotations were unconstrained at the global/local boundary nodes. In LBC2, the w-displacements were unconstrained except a small portion (Γ_1) near the middle of the boundary, whereas these were constrained at all boundary nodes in LBC3.

Figures 9 and 10 show the contour plots of the wrinkle displacements for the considered boundary conditions for 10 μm and 2 μm thickness models. As can be seen in the figures, the wrinkle contours were almost indistinguishable regardless of the boundary conditions considered for the two models with different thicknesses. The comparison of the w-displacements along AA' line was plotted in Fig. 11 for the 10 μm thickness model. For better viewing, the figure was plotted for a tightly zoom portion which corresponds to the second quarter of the AA' line shown in Fig. 6. The figure showed a very good agreement with all three curves falling on top of each other. There occurred slightly more differences for the 2 μm thickness model as shown in Fig. 12; however, these were not significant. These results suggested that prescribing w at the global/local boundary would not be significant for partly wrinkled membrane problems, as long as one modeled the local mesh to include the wrinkled region, and thus the global/local boundary to be reasonably away from it.

D. Load Level Effect

Next, the effect of applied load level was investigated. Figure 13 compares the wrinkle pattern for the 10 μm thickness membrane. Figure 13b shows the wrinkle contour for the current load set of $T_1 = 22.5$ N and $T_2 = 30$ N, and Fig. 13a for the reduced load set of $T_1 = 22.5$ N and $T_2 = 3$ N. For the reduced load set, a very slight amount of the out-of-plane displacements occurred, which could be considered as a nucleation of wrinkling. In the figure, even the geometric imperfection seeded initially to instigate the buckling was visible.

Similar computations were done for the 2 μm thickness membrane. In this case, the wrinkling deformation occurred even under a very small load level as shown in Fig. 14. However, as the loads were decreased, the wrinkle pattern became much simpler with a fewer number of wrinkles. The wrinkle height also decreased.

V. Conclusion

A global/local analysis strategy was developed to calculate detailed wrinkle deformation of partly wrinkled thin membranes.

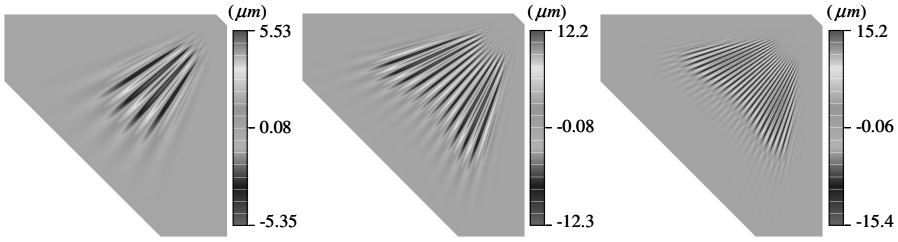

a) b) c)

Fig. 14 Contour plots of wrinkle displacements at different load levels for 2 μm thickness model: a) $T_1 = 0.045$ N, $T_2 = 0.06$ N; b) $T_1 = 0.45$ N, $T_2 = 0.6$ N; and c) $T_1 = 4.5$ N, $T_2 = 6$ N.

First, the in-plane solutions were obtained from a global membrane analysis with a relatively coarse mesh. Next, the global solution was used to derive boundary conditions of the local problem where detailed wrinkled shape was calculated by a geometrically nonlinear post-buckling analysis. In the global analysis, membrane elements were used with wrinkle algorithm based on a penalty-parameter modified material model. In the local analysis, the wrinkle deformation was calculated with shell element meshes seeded with random geometric imperfections.

The global/local analysis procedure was applied to a corner-loaded square membrane, and it was found that the mixing of membrane and shell analyses in the global/local context was an efficient way to calculate the wrinkle deformation while saving huge computational resource. The accuracy of the global/local procedure was established by comparing the results with those of conventional shell analysis, and the mesh convergence and global/local boundary conditions were also studied. The effect of membrane thickness and the applied load level on the wrinkling was investigated. It was found that more complex wrinkle pattern with larger number of wrinkles was resulted in as the membranes became thinner and the loads were higher, where highly refined meshes were required to model the fine details of wrinkle deformation.

Acknowledgments

The work described in this paper was funded in part by the In-Space Propulsion Technology Program, which is managed by NASA's Science Mission Directorate in Washington, D.C., and implemented by the In-Space Propulsion Technology Office at Marshall Space Flight Center in Huntsville, AL.

References

[1] Roddeman, D. G., Drukker, J., Oomens, C. W. J., and Janssen, J. D., "The Wrinkling of Thin Membranes: Part 1—Theory," *Journal of Applied Mechanics*, Vol. 54, No. 4, 1987, pp. 884–887.

[2] Roddeman, D. G., Drukker, J., Oomens, C. W. J., and Janssen, J. D., "The Wrinkling of Thin Membranes: Part 2—Numerical Analysis," *Journal of Applied Mechanics*, Vol. 54, No. 4, 1987, pp. 888–892.

[3] Roddeman, D. G., "Finite-Element Analysis of Wrinkling Membranes," *Communications in Applied Numerical Methods*, Vol. 7, No. 4, 1991, pp. 299–307.

[4] Muttin, F., "A Finite Element for Wrinkled Curved Elastic Membranes, and Its Application to Sail," *Communications in Applied Numerical Methods*, Vol. 12, No. 11, 1996, pp. 775–785.

[5] Kang, S., and Im, S., "Finite Element Analysis of Wrinkling Membranes," *Journal of Applied Mechanics*, Vol. 64, No. 2, 1997, pp. 263–269.

[6] Lu, K., Accorsi, M., and Leonard, J., "Finite Element Analysis of Membrane Wrinkling," *International Journal for Numerical Methods in Engineering*, Vol. 50, No. 5, 2001, pp. 1017–1038.

[7] Miller, R. K., Hedgepeth, J. M., Weingarten, V. I., Das, P., and Kahyai, S., "Finite Element Analysis of Partly Wrinkled Membranes," *Computers and Structures*, Vol. 20, Nos. 1–3, 1985, pp. 631–639.

[8] Miyazaki, Y., and Nakamura, Y., "Dynamic Analysis of Deployable Cable-Membrane Structures with Slackening Members," *Proceedings of the 21st International Symposium on Space Technology and Science*, Vol. 1, Omiya, Japan, 1998, pp. 407–412.

[9] Liu, X., Jenkins, C. H., and Schur, W., "Large Deflection Analysis of Pneumatic Envelopes Using a Penalty Parameter Modified Material Model," *Finite Elements in Analysis and Design*, Vol. 37, No. 3, 2001, pp. 233–251.

[10] Wong, Y. W., Pellegrino, S., and Park, K. C., "Prediction of Wrinkle Amplitudes in Square Solar Sails," AIAA Paper 2003-1982, 2003.

[11] Su, X., Abdi, F., Taleghani, B., and Blandino, J. R., "Wrinkling Analysis of a Kapton Square Membrane Under Tensile Loading," AIAA Paper 2003-1985, 2003.

[12] Tessler, A., Sleight, D. W., and Wang, J. T., "Nonlinear Shell Modeling of Thin Membranes with Emphasis on Structural Wrinkling," AIAA Paper 2003-1931, 2003.

[13] Murphey, T. W., Murphy, D. M., Mikulas, M. M., and Adler, A. L., "A Method to Quantify the Thrust Degradation Effects of Structural Wrinkles in Solar Sails," AIAA Paper 2002-1560, 2002.

[14] Murphy, D. M., and Wie, B., "Robust Thrust Control Authority for a Scalable Sailcraft," AAS Paper 04-285, 2004.

[15] Hirai, I., Uchiyama, T., Mizuta, Y., and Pilkey, W., "An Exact Zooming Method," *Finite Elements in Analysis and Design*, Vol. 1, April 1985, pp. 61–69.

[16] Jara-Alamonte, C., and Knight, C., "The Specified Boundary Stiffness/Force SBSF Method for Finite Element Subregion Analysis," *International Journal for Numerical Methods in Engineering*, Vol. 26, No. 7, 1988, pp. 1567–1578.

[17] Woo, K., and Whitcomb, J. D., "Global/Local Finite Element Analysis for Textile Composites," *Journal of Composite Materials*, Vol. 28, No. 14, 1994, pp. 1305–321.

G. Agnes
Associate Editor